JOURNAL OF MATERIALS SCIENCE 14 (1979) 321–332

# The resistance to crack growth of asbestos cement

J. C. LENAIN, A. R. BUNSELL
*Ecole Nationale Supérieure des Mines de Paris, Centre des Matériaux BP 87 91003 Evry Cédex, France*

The crack resistance of sheet asbestos cement has been characterized in terms of an $R$-curve which can accomodate effects which often influence the measurement of the critical stress intensity factor $K_c$. The detection and location of the acoustic emission (AE) obtained from the asbestos cement has shown that it originates from microcracks in a zone just in front of the crack. The size of this zone increases to a maximum during slow propagation of the major crack and afterwards remains of constant size during the final crack growth. The form of the $R$-curve has been explained in terms of the mechanisms of fracture with the aid of AE and fractography studies. An analytical study has related the experimental $R$-curve to a theoretical $R$-curve and, hence, to the volume fraction, fibre aspect ratio and the strength of the fibre–matrix interface. It has been shown that the microcracking zone can be considered as a theoretical extension, of about one third of the zone length, to the real crack length.

## 1. Introduction

The ultimate tensile strength, resistance to impact and ability to inhibit cracking in a brittle material such as cement can be increased by the addition of short fibres such as those of asbestos or glass. Although at present the subject of considerable controversy, asbestos cement, particularly in the form of thin plates such as corrugated roofing, is widely used and is likely to continue to be used. In this form the asbestos fibres allow thinner sheets to be made and it is the ability of the asbestos fibres to inhibit crack propagation in this type of material which has been the major interest of this study.

The toughness of the asbestos cement is an important parameter and although the material is inhomogeneous, containing many defects such as microcracks, holes and discontinuities, it has previously been shown that cement behaves as an elastic medium to which a fracture mechanics approach to the study of its cracking is valid [1]. Cooper and Figg [2] have demonstrated the influence of water in cement paste as they found that values for the work to fracture varied from 12 to 15 $J m^{-2}$ as the cement was dried. For asbestos cement it has been shown [3] that its modulus falls with increasing porosity and fibre volume fraction whilst its strength passes through a maximum at about an 8% volume fraction. A study [4] of cement reinforced by glass fibres has indicated a continuously increasing work of fracture by impact with increasing volume fraction.

A recapitulation of the main ideas of linear elastic fracture mechanics which will be drawn upon during this paper seems worthwhile at this point in order to clarify the argument presented later.

It was shown as long ago as 1913 by Inglis [5] that the nominal stress ($\sigma_0$) applied to a body in a direction normal to the axis of a crack or notch, considered as being elliptical, is magnified and attains a value of

$$\sigma = \sigma_0 2\left(\frac{a}{\rho}\right)^{1/2} \quad (1)$$

in which $a$ is half the crack length and $\rho$ the radius of curvature of the crack tip. The ratio $\sigma/\sigma_0$ is called the stress concentration coefficient. This coefficient depends only on the geometry of the specimen and the load applied. In an ideally elastic

case when $\sigma_0$ reaches the value $\sigma_c$ necessary to separate the structure the crack will propagate. Griffith [6] showed from energetic considerations that $\sigma_c$ could be related to a physical property of the material, the surface energy ($\gamma$), by the relation

$$\sigma_c = \sqrt{(E\gamma/a)} \tag{2}$$

in which $E$ is Youngs modulus.

The factor $\gamma$ is usually increased by plastic deformation by a factor which we can write $\gamma_p$. In order to have maximum energy absorbed during fracture, that is to have greatest toughness, $\sqrt{(\sigma_c^2 a)}$ should clearly be as great as possible and this factor is known as the stress intensity factor $K$. For a specimen of finite size it is necessary to introduce a correcting geometrical factor $Y$ so that

$$K = Y\sigma(a)^{1/2}. \tag{3}$$

When the value of $K$ exceeds a limit denoted by $K_c$ which depends on the properties of material, the crack becomes unstable and propagates.

Irwin [7] was able to relate the rate of release of energy from the body ($G$) to the factor $K_c$ and show that

$$K_c^2 = E^* G_c \tag{4}$$

where $E^* = E$ in the plane stress situation and $E/(1 - \nu^2)$ in plane strain where $\nu$ is Poisson's ratio.

Dugdale and Barenblatt [8] in considering the effect of plastic deformation at the root of the notch added a theoretical extension to the crack of length equivalent to the length of the plastic zone. This extension was considered to experience a closing stress which in reality accounted for the limiting of the maximum stresses by plastic deformation.

These approaches have all originated from considerations of the rupture of an infinite medium whereas practical considerations very often necessitate tests on relatively small specimens. Although correcting factors can be applied to the above equations, all too often the parameters measured are no longer solely material properties but are influenced by the geometry of the specimen, its size and its thickness. Whilst the testing of very large specimens is not always impossible many applications demand that the material be used in what from the theoretical point of view are too small dimensions. It is because of these limitations of linear elastic fracture mechanics that this study has attempted to characterize the material in terms of resistance or $R$-curves.

With many fragile materials, given favourable loading conditions, the development of a fracture consists of an initial slow stable growth followed by a sudden unstable run of the fracture which then stops. Taking the thermodynamic argument of Griffith, the unstable advance occurs when the rate of energy ($u$) released by the body is equal to or greater than the energy ($S$) required to create the new fracture surfaces so that we can write

$$\frac{\partial}{\partial a}(u - S) \geqslant 0 \tag{5}$$

by putting $G = \partial u/\partial a$ and $\partial S/\partial a = R$, we can write this equation as

$$G - R \geqslant 0. \tag{6}$$

Kraft *et al.* [9] have postulated that for a given material and thickness there is a unique relationship between the growth of the crack and the factor of resistance $R$. This relationship is represented by a curve of resistance to crack growth or $R$-curve.

Fig. 1 shows schematically the variation of $K^2/E$ with crack length at different applied loads. On the same graph is traced the $R$-curve for that material with a given crack length. It can be seen that the difference $G - R$ is favourable for crack propagation between $a_0$ and the point of intersection of the two curves. In the cases of the applied loads $\sigma_1$ and $\sigma_2$ crack propagation is arrested as it passes into a zone in which $G - R$ is negative. With the stress $\sigma_3$ however, the two curves are tangential and it is at their point of

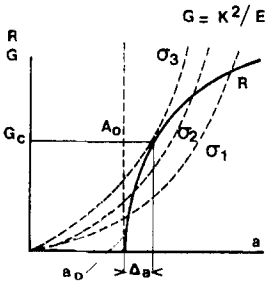


*Figure 1* The relationship between the $R$-curve and the energy available for crack propagation. Crack propagation stops for stresses $\sigma_1$ and $\sigma_2$ but is not arrested for the limiting case $\sigma_3$.

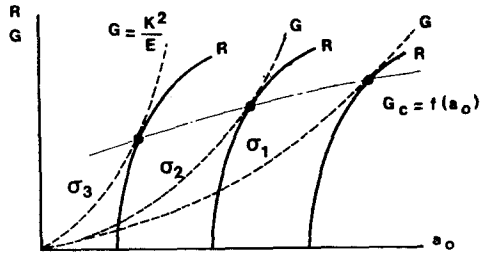


*Figure 2* Effect of notch length on the value of $G_c$.

contact with a crack growth of $\Delta a$ that the crack becomes unstable.

If it is not possible to assume that the form of the $R$-curve is not altered by the initial crack length, Fig. 2 shows the influence of notch length on the value of $G_c$. In general it is necessary to add other energy-absorbing mechanisms to those in Equation 4, such as the kinetic energy $C$ dissipated, the work $w_F$ done by the external loading agent and the plastic deformation $w_p$, so that Equation 5 becomes:

$$\frac{\partial}{\partial a}(u + C + w_F - S - w_p) \geqslant 0 \qquad (7)$$

If the left-hand side of this equation is positive, or zero, crack growth will occur and will stop if it becomes negative. Bluhm [10] has examined the possibilities of the arrest of cracks after the initial propagation by the effects of the specimen geometry, the form of the $R$-curve and the type of loading.

An $R$-curve then is the resistance of the material, in terms of energy absorbed, to crack propagation. This can be obtained by reference to Equation 3 which with the aid of Equation 4 can be rewritten

$$G = \sigma^2 Y^2 a/E$$

or in terms of the compliance $c$ of the material it can be shown that

$$G = \frac{1}{2}\frac{P^2}{b}\frac{\partial c(a)}{\partial a} \qquad (8)$$

where $b$ is the thickness of the specimen and $P$ is the load at which the crack propagates.

From Equation 4 we can now deduce that

$$2\frac{Y^2}{E}\frac{a}{w} = bW\frac{\partial c(a)}{\partial a} \qquad (9)$$

where $W$ is the width of the specimen.

In order to draw the $R$-curve it is necessary to refer to Equation 8 and know the load at which crack propagation starts at every value of crack length.

The $R$-curves obtained seems to be independent of the specimen geometry and are a function only of the thickness, the speed of crack propagation and the temperature, so may be considered as characteristic of the material tested in much the same way as $K_c$ is used for completely brittle materials. This is particularly interesting for this study as Brown has shown that although the stress intensity factor ($K_c$) is independent of the geometry and fracture length in cement paste [1] this is not the case with glass fibre reinforced cement [11]. By extrapolating back it is possible to see from Brown's results that although the fibres inhibited the crack growth they did not prevent crack initiation as the value of $K_c$ for a zero crack length was of the same order as that of the cement paste.

Under tensile loading it is found that asbestos cement has a more linear and elastic response than the glass fibre reinforced cement of Brown's study and this should lead to greater ease in applying the ideas of fracture mechanics to it.

## 2. Materials

The material which was studied was Portland cement reinforced by asbestos fibres randomly distributed in the plane of the sheets used. The fibres, which are closer to a fibrillar bundle than single fibres, generally have dimensions of several millimetres length and diameters of around 25 $\mu$m. Specimens were cut from industrially manufactured flat sheets having a thickness of 6.3 mm. The fibre volume fraction ($V_f$) was 0.054, the ratio by weight of water to cement was 0.3 and all tests were conducted on material aged for one year.

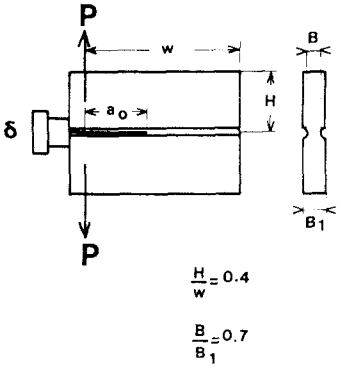


*Figure 3* Specimen geometry.

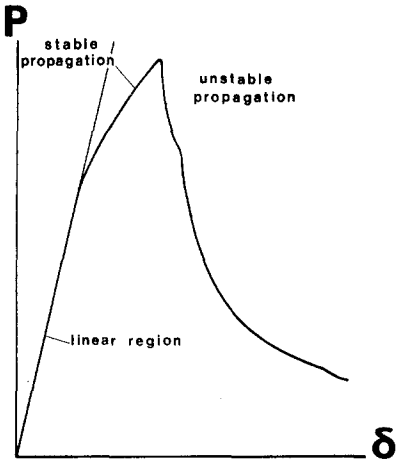


*Figure 4* Typical curve of load COD for a CT specimen of asbestos cement.

## 3. Apparatus and experimental techniques

The compact tension (CT) form of specimen which was used in this study is illustrated in Fig. 3. In order to guide the fracture, side grooves were machined into the sample thereby reducing the thickness by 30%. The notch root was cut with a 0.4 mm jeweller's saw. Displacement was measured by an extensometer over a 20 mm gauge length and tests were conducted in an Instron tensile machine.

A Dunegan-Endevco acoustic emission system 3000 with an amplification of 90 dB was used to monitor internal mechanisms of deformation during loading.

The transducer had its primary resonance at 230 kHz and a system of filters restricted the signals processed to those falling in the range 100 to 300 kHz. A module 920 used as a linear localizer and employing two transducers permitted the location of the source of the emission.

## 4. Experimental results

Fig. 4 shows a typical load–elongation curve, for a CT specimen exhibiting three distinct stages: (a) a linear region; (b) a non linear region representing stable, slow crack growth visible to the naked eye. During this stage asbestos fibres could be seen bridging the crack, see Fig. 5; (c) a discontinuous unstable crack growth region.

The crack length was determined by a compliance method. As can be seen from Fig. 6, the compliance curves obtained with a notched specimen and a semifractured specimen in which fibre bridges could be seen, were identical and their slope agrees with that calculated for an isotropic material using Equation 9. On unloading however the semifractured specimens showed a residual opening displacement ($\delta r$) which could be related to the crack length (Fig. 7). This residual opening, which did not occur with notched specimens was due to the partially pulled out fibres in the region of the crack.

In order to draw the $R$-curve, the following were necessary: a graph of load against crack opening displacement $\delta$; the choice of an increase in crack size $\Delta a_n$; with the help of specimen curves and knowing the residual opening displacement $\delta r_n$, the calculation of the compliance $C_n$ of the specimen at all points of the curve; and the calculation of the stress intensity factor $K_r$ at each point on the load–extension graph by determining the compliance (inset sketch of Fig. 6).

With the CT form of specimen crack propagation was relatively stable and by repeating these operations $N$ times a series of values was obtained for $K_r$ and $a$ from which it was possible to draw all of the $R$-curve. As Fig. 8 shows schematically, there were three distinctive stages in the curve after crack growth had initiated. During the

*Figure 5* Asbestos fibres bridging the major crack.

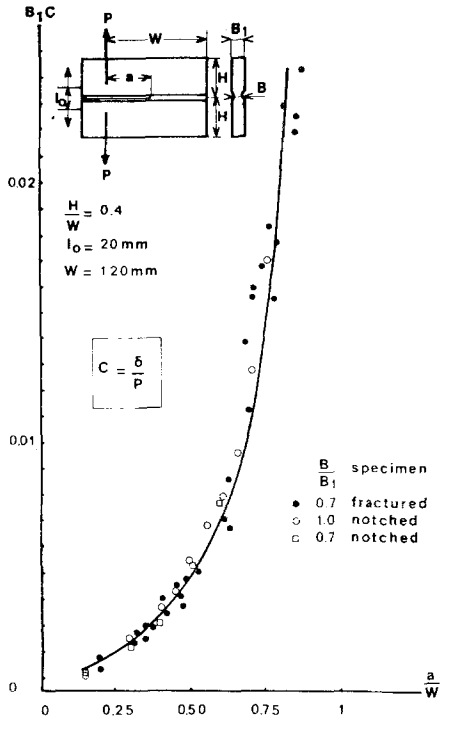


*Figure 6* Change of compliance with notch depth.

initial propagation stage, over a length $a_1$ which was of the order of 4 mm, the resistance $R$ increased steeply with crack growth. The second stage was characterized by a reduction in the rate of increase of $R$ until a crack length $a_2$, about 15 mm, was attained. After this point the resistance to propagation $R$ remained constant during crack propagation.

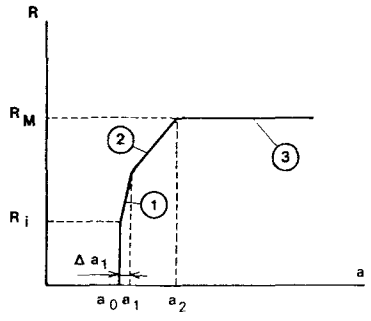


*Figure 8* Schematic representation of the $R$-curve for asbestos cement.

In order to investigate the effect of initial crack length on the $R$-curves a series of specimens was tested and the curves obtained for each. As Fig. 9 indicates although the $R$-curves are not identical the value of $K_i$, the coefficient of stress intensity at crack initiation, is sensibly constant for ranges of $a_0/W$ between 0.3 and 0.6. As Brown [11] has pointed out for glass reinforced cement the value of $K_c$ at the point of unstable crack growth is not constant for asbestos cement.

The specimen width was found to have no influence in the testing specimen for the range 120 to 240 mm.

Not all the $R$-curves obtained were smooth as is shown by Fig. 10 and these irregularities were associated with sudden unstable crack growth followed by the arrest of the crack. It is clear then that the form of the $R$-curve for asbestos cement is dependent on the speed of crack propagation. To study the influence of speed a series

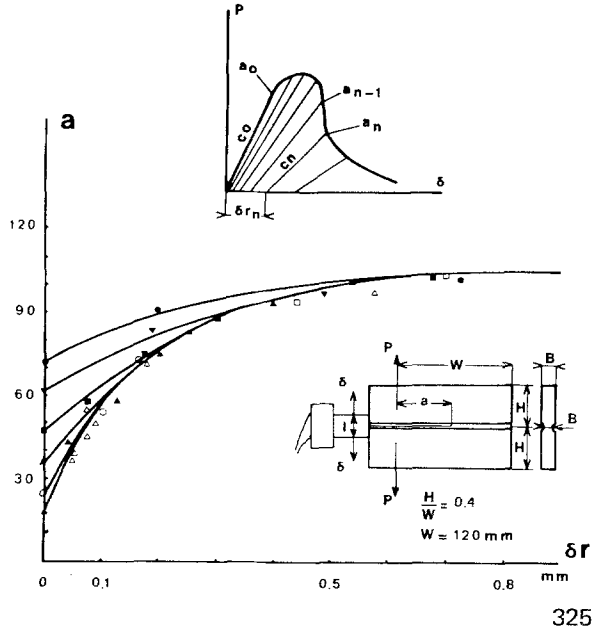


*Figure 7* Relationship between crack length and residual crack opening displacement.

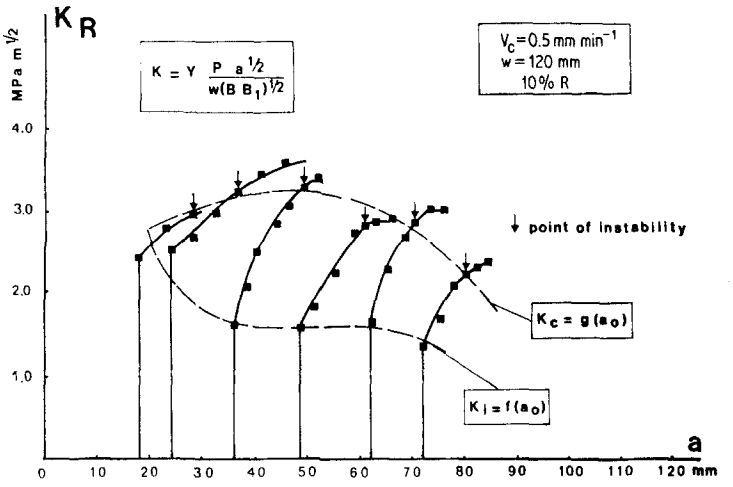


*Figure 9* Influence of the initial notch length $a_0$ on the $R$-curve.

TABLE I Effect of the Instron cross-head speed on the speed of crack propagation at the beginning of stable crack growth and on $K$ at the point of non-linearity. Values for tests carried out at 21% r.h.

| $K_i$ (MPa m$^{1/2}$) | $\dot{a}_2$ (mm sec$^{-1}$) | $V_c$ (cm min$^{-1}$) |
|---|---|---|
| 1.67 | 0.055 | 0.05 |
| 1.71 | 0.1 | 0.01 |
| 1.74 | 0.2 | 0.02 |
| 1.68 | 0.3 | 0 05 |
| 1.88 | 0.5 | 0.1 |
| 1.71 | 1.9 | 0.2 |
| 1.71 | 4.5 | 0.5 |

of identical specimens was tested at loading speeds between 0.005 and 0.5 cm min$^{-1}$. Table I shows the relationship between the speed of loading ($V_c$) the speed of crack growth ($\dot{a}_2$) and the factor $K_i$. It can be seen that within experimental limits $K_i$ remains constant. The gradient of the first zone shown in Fig. 8 $(\partial R/\partial a)_1$ does depend however on the speed as Fig. 11 shows, although that of the second zone $(\partial R/\partial a)_2$ is insensitive to the speed. These tests were conducted with the material in three states of humidity and as can be seen in Fig. 11 the presence of free water in the cement lowers the resistance to fracture and increases the speed of propagation in the first zone of the $R$-curve.

In order to obtain a better understanding of the processes involved in the fracture of asbestos cement we have monitored the acoustic emissions during loading. It has been shown that acoustic emission started before the point of non-linearity in the curve shown in Fig. 1 was reached. Here the total number of acoustic events varied as is shown in Fig. 12 and it was found possible to fit an equation relating the number of emissions to the sixth power of the stress intensity factor $K$ to this curve. It was important to find out from where this noise was coming as possible sources

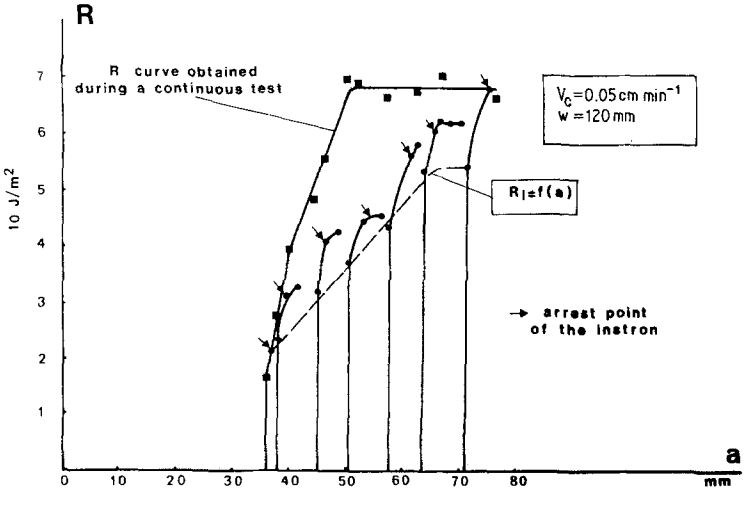


*Figure 10* Effect on the $R$-curve of cycling the specimen to continually increasing loads, each cycle returning to zero load, compared to that obtained during a simple continuous test. The crack was seen to continue to propagate in an unstable manner each time the Instron cross-head was stopped.

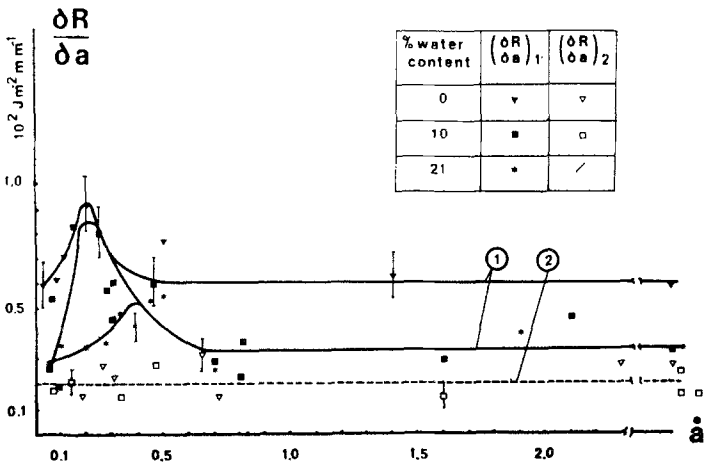


*Figure 11* Influence of the speed of crack growth on the $R$-curve.

included the loading pins through the specimen, the specimen body in general or the region of the notch root where stresses were highest.

For this we used a method of location for the acoustic emissions involving two transducers placed either side on a line normal to the axis of the crack or along the crack axis on either side of the crack root. For these experiments the displacement rate of the Instron cross-head was 0.05 cm min$^{-1}$ and an extensometer was used to measure the crack opening displacement (COD).

With the transducers placed on a line normal to the crack axis it was shown that about 80% of the emissions came from a very narrow band just in front of the crack tip. The remaining 20% most probably came from the region of the loading pins.

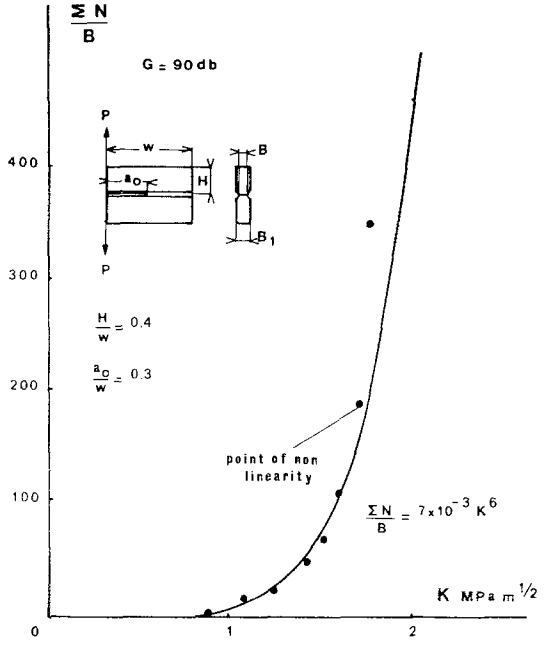


*Figure 12* Acoustic emission as a function of $K$.

In order to determine the size of the zone in front of the crack in which the emissions were originating, the transducers were then placed along and on either side of the line of crack propagation. In this way it was possible to record the length of the zone around the crack tip which was actively emitting. At the point of non-linearity in the load–elongation curve, the length of the actively emitting zone ($Z_i$) was 12 mm. The length of this zone in front of the crack increased continuously as the crack propagated in a stable fashion and the zone reached a maximum length of 28 mm near to the maximum load at Point 1 in Fig. 13. At this point the Instron machine stopped and the crack was seen to advance rapidly and then stop with a constant COD. The specimen was then unloaded and reloaded so as to verify the crack length by the compliance method. The test was continued and the specimen was reloaded to the maximum load associated with the new crack length. The crack advanced to Point 3 after stopping the machine at Point 2. This operation was repeated several times with acoustic emission being used to detect the propagation and arrest of the crack. At each of the three different crack lengths studied, the distances between the edge of the disturbed crack zone and the visible crack tip was found to be 28, 29 and 27 mm, respectively. This showed that the volume of the acoustically active zone remains constant during the stage of unstable crack propagation. It can be seen then that ahead of a crack in asbestos cement there is a region of microcracks created before the point of non-linearity in the stress–strain curve. The size of the zone increases progressively during the stage of stable crack propagation reaching a maximum

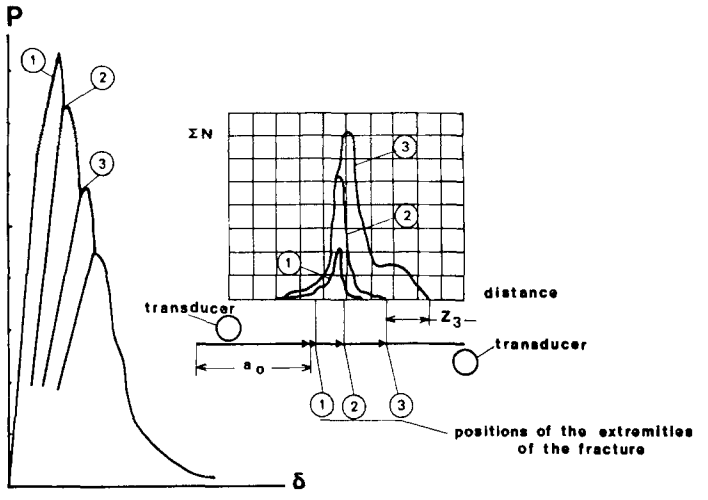


*Figure 13* Location of acoustic emission during each crack propagation.

value near to the maximum load. The size of the zone of microcracks remains constant, however, during the period of unstable crack propagation.

When the sample was reloaded after initial loading and visible crack propagation, acoustic emissions were recorded before the previous load level at which the crack arrested was reached.

The Kaiser effect is therefore not found in this type of material. The location technique showed that on unloading the asbestos cement, emissions were produced which originated from the region of the whole visible crack but not from the zone of microcracks.

It is clear that these emissions originate from asbestos fibres which are exposed by the major crack and partially pulled out of the cement matrix. During the unloading of the specimen these fibres are damaged and particles of cement attached to them are crushed thus giving rise to emissions.

The efficiency of these damaged fibres for resisting further opening of the crack during a subsequent loading is obviously reduced. Because of this the crack starts to propagate during reloading at a lower stress level than in the preceding cycle, see Fig. 10. Accordingly, after a previous loading, emissions are detected before reaching the previous crack arrest load in asbestos cement.

## 5. Discussion

The detection and location of the acoustic emissions have shown clearly that there are a number of stages involved in the fracturing of a notched specimen of asbestos cement. These stages are shown in Fig. 14 and are as follows:

(a) In the elastic region of the stress–strain

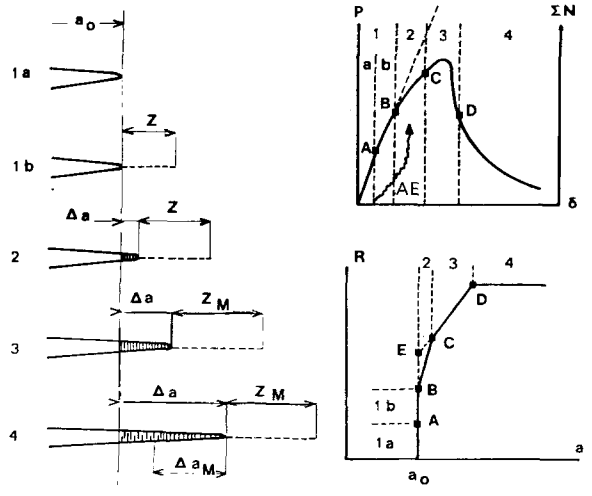


*Figure 14* The mechanisms of crack growth with the development of a zone (z) of microcracking ahead of a major crack and the development of fibre bridges across the crack.

curve from Point A there is a zone of microfissures created at the tip of the crack (Figs. 13 and 14). The stress intensity factor associated with the creation of this region we shall designate as $K_0$.

(b) At the point of non-linearity (Point B) the zone of microcracking attains a size $Z_i$ and the crack begins to propagate slowly.

(c) During this period of stable propagation, which it is possible to follow by eye, the zone of microcracking ahead of the crack increases in size until Point C is reached after which it remains constant.

During the propagation of the crack it was possible to observe the pull out of asbestos fibres from the cement matrix at the fracture surface. Usually it was the fibre–matrix interface which was seen to have given way although occasionally a bundle of asbestos fibres would pull out still enrobed in cement showing that shear failures of the matrix around the fibre can take place.

In terms of the $R$-curves it is clear that a zone of microcracking in front of the crack, and the fibres which bridge it, increase the resistance of the material to crack propagation. These two mechanisms supplement each other at the beginning of slow crack propagation but after Point C, at which the zone of microcracking has attained its maximum size, it is the fibre bridges which account for the continuing increase in resistance. At Point D the opening of the crack corresponds to a maximum length of fibre-bridged crack giving the maximum resistance to propagation. From that point the resistance of the material to cracking is constant.

It is now possible to see how this description of the fracture processes also account for the speed effects described earlier. In the regime between Points C and D in Fig. 4, the speed of crack propagation ($\dot{a}_3$) is also the speed of the zone of microcracking, including its boundary. This speed is then the speed of the most advanced border of the microcracking zone. In Zone 2 the crack tip is moving at a speed $\dot{a}_2$ which is less than $\dot{a}_3$, the speed of the extremity of the microcrack region. The rate of growth of the microcrack zone is therefore related to $\dot{a}_3 - \dot{a}_2$ as is the gradient of the $R$-curve $(\partial R/\partial a)_1$. As $(\partial R/\partial a)_1$ depends on $\dot{a}_2$ it will similarly be a function of the specimen geometry and the speed of loading.

If the speed of crack propagation becomes greater than the speed $\dot{a}_3$ the size of the zone of microcracking will decrease and with it the resistance $R$ of the material. This will result in changes or irregularities in the $R$-curve obtained.

## 6. Theoretical model

During crack propagation the fibres which bridge the fracture inhibit its opening and contribute a factor $(K_r)$ to the stress intensity factor $(K_R)$ necessary to cause crack propagation. We can therefore write

$$K_R = K_0 + K_r \tag{10}$$

where $K_0$ is the stress intensity factor of the matrix in the absence of the fibres. This model is analogous to that of Dugdale's [8] accounting for the effect of plastic deformation ahead of a crack in a metal. Paris [12] has proposed an analytical expression to calculate the additional stress intensity factor $(K_i)$ when there is a uniform pressure $p$ applied to the crack tip, see Fig. 15.

$$K_i = \frac{pa^{1/2}}{\pi^{1/2}}\left[\sin^{-1}\frac{c}{a} - \sin^{-1}\frac{b}{a} - \left(1-\frac{c^2}{a^2}\right)^{1/2} + \left(1-\frac{b^2}{a^2}\right)^{1/2}\right]. \tag{11}$$

From this equation it is possible to calculate the role of each type of mechanism, given certain conditions. It is necessary to assume that the closing stresses produced by the asbestos fibres are the same for microcracks as for the main crack. It is assumed that a zone of microcracking of size $Z$ can be represented by an imaginary linear increase of crack length of $z = \alpha Z$, where $\alpha$ is a factor less than unity, to which the closing stress is uniformly applied.

We can now rewrite Equation 10 as

$$K_R = K_0 + \frac{p}{\sqrt{\pi}}(a+\alpha Z)^{1/2}\left\{\frac{\pi}{2} - \sin^{-1}\frac{a_0}{(a+\alpha Z)} + \left[1+\frac{a_0^2}{(a+\alpha Z)^2}\right]^{1/2}\right\} \tag{12}$$

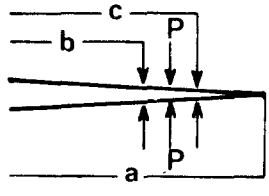


*Figure 15* Model proposed in which the bridging fibres are replaced by a uniformly distributed closing pressure $p$.

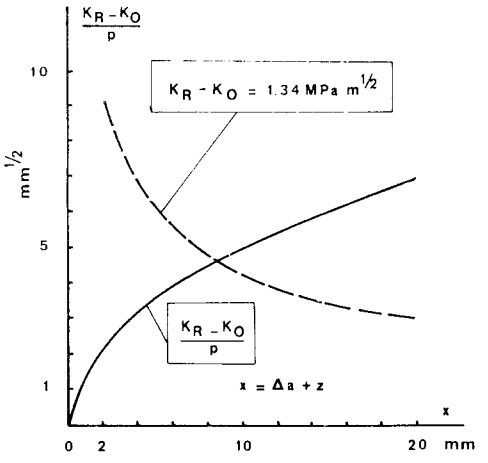


*Figure 16* Theoretical curves of $(K_R - K_0)/p$ against crack size together with the variation of $p$ given the value of $K_R - K_0$ obtained experimentally corresponding to a maximum contribution of the zone of microcracking with no effect of fibre bridges.

in which $a_0$ is the original crack length and $a = a_0 + \Delta a$ in which $\Delta a$ is the measurable crack extension.

It is now possible to draw a theoretical curve of $(K_R - K_0)/p$ against $x = (\Delta a + z)$ as shown in Fig. 16. The experimentally obtained curve, represented by Fig. 14, gives the maximum resistance of the material to cracking without crack propagation. That is the sum of the maximum contribution of the zone of microcracking and the fibre bridges. This value is given by Point E and reveals the relationship between $p$ and the imaginary additional crack length $z_m$. This is the second dotted curve shown in Fig. 16 although the ordinate $x$ should be read with $\Delta a$ as zero. The value of $p$ and hence $z_m$ is obtained by successive approximations of Equation 12 to give the same gradient in the region CD for the theoretical curve as found in practice. This is shown in Fig. 17. The experimental curve, which it should be recalled is a function of the actual major crack length and the displacement of the two curves, is due to the effect of the zone of microcracks. It can be seen that from Point C the two curves are parallel so that the translation of the curves parallel to the abscissa is equal to $z_m$.

The location of the acoustic emission has revealed that the lengths of the zone of microcracking at the points of non-linearity of the stress–strain curve and at its maximum size, $Z_i$ and $Z_m$ are respectively 12 mm and 28 mm. As the rate of increase in size of the zone is proportional to the difference of speeds of the crack tips $(\dot{a}_2)$ and the zone frontier $(\dot{a}_3)$ the increase of imaginary crack length can be written

$$\Delta z = \frac{(\dot{a}_3 - \dot{a}_2)}{\dot{a}_2} \Delta a \qquad (13)$$

with $\Delta z = z - z_i$ and $z = z_m$ at $\Delta a = \Delta a_1$.

A comparison of the experimental and theoretical curves shown in Fig. 17 allows the following expressions to be written for the experimental curve

$$K_R = K_i + \chi \Delta a$$

for the theoretical curve

$$K_R = K_i + \beta(\Delta a + z - z_i).$$

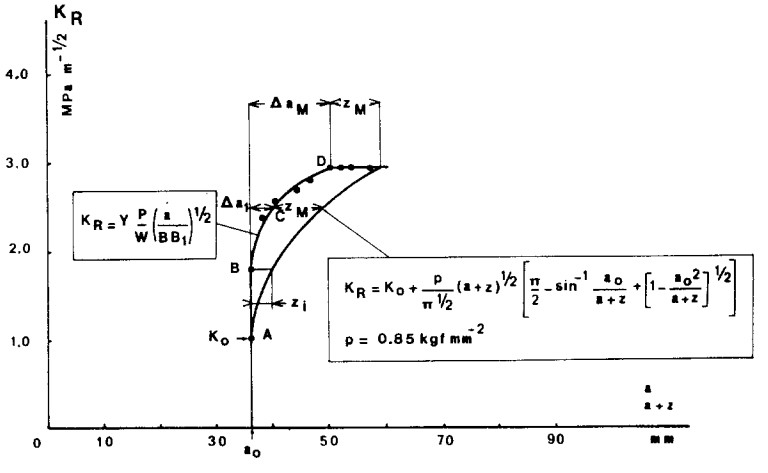


*Figure 17* Comparison of the $R$-curves obtained experimentally and theoretically. The displacement is due to the contribution of the zone of microcracks which is accounted for in the theoretical curve but not measured experimentally.

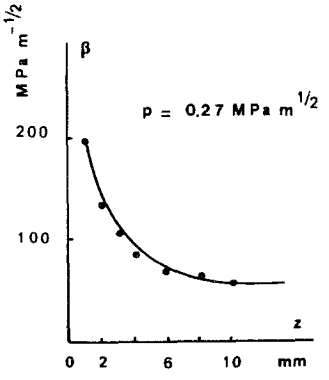


*Figure 18* Influence of the zone of microcracks at the point of initiation of crack propagation on the gradient of the $R$-curve.

If the curves were considered to be linear in the second region, $\chi$ and $\beta$ would be their gradients so that it is possible to write

$$\chi = \beta\left(1 + \frac{z - z_i}{\Delta a}\right) = \frac{K_R - K_i}{\Delta a} = \frac{\partial K_R}{\partial a} \quad (14)$$

and from Equation 13

$$\frac{\partial K_R}{\partial a} = \beta \frac{\dot{a}_3}{\dot{a}_2} . \quad (15)$$

The initial gradient of the experimentally obtained $R$-curve is therefore related to the ratio of the speeds and the gradient of the analytical $R$-curve at the point $(a_0 + z_i, k_i)$. Fow low values of $z$, $\beta$ is a function of $z$ as is shown in Fig. 18 and the results shown in Fig. 19 indicate values of $z_i$ between 3 and 6 mm giving typical values of: $z_i = 3.8$ mm and $z_m = 11.2$ mm. A direct comparison, using Fig. 17, gives similar results of $z_i = 3.5$ mm and $z_m = 10$ mm. From the acoustic emission results $\alpha Z$ was found to be of the order of 12 mm and $\alpha Z_m$ about 28 mm, giving a value

$$\alpha \approx \tfrac{1}{3}.$$

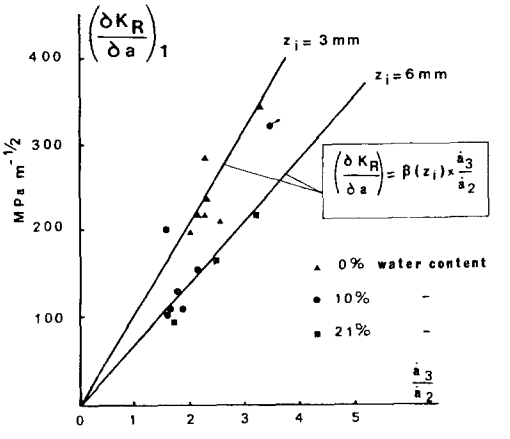


*Figure 19* Relationship between the initial gradient of the $R$-curve and the ratio of the speeds of crack propagation.

The pressure $p$ is a function of the strength of the fibre matrix interface ($\tau$), the fibre aspect ratio, the volume fraction and an efficiency factor ($\eta_\theta$) which is due to the fibre arrangement [13] so that

$$p = \eta_\theta V_f \tau \frac{l}{d} \quad (16)$$

With an aspect ratio of about 200 and a resulting pressure of 8.5 MPa (as obtained from Fig. 17), a value of 2.0 MPa is obtained for $\tau$ which is in good agreement with the values for interfacial strength which are 0.8 and 3 MPa [14].

## 7. Conclusions

It is possible to distinguish three stages of crack growth in asbestos reinforced cement:

(a) The creation of a zone of microcracks in front of the main crack during the elastic region of the stress–strain curve.

(b) The growth of this zone together with a slow stable growth of the crack.

(c) Propagation of the crack with the size of the zone of microcracks remaining constant.

The fibres which bridge the microcracks as well as those across the main crack induce a closing stress on the tips of the cracks and so increasing the work of fracture of this material. It has been possible to explain the form of the $R$-curves in terms of these mechanisms and also to develop an analytical theory to account for the results obtained. A linear extension of the crack into the zone of microcracks has been imagined and this accounts for the observed behaviour if a closing pressure provided by the bridging fibres is exerted. The $R$-curve determined in this way depends solely on the intrinsic characteristics of the composite which are the crack resistance of the matrix in the presence of fibres, volume fraction, strength of the fibre cement interface and the aspect ratio of the fibre, and so itself can be considered as characteristic of the material.

## Acknowledgement

The author would like to thank the company

EVERITUBE for their support and the supply of materials for this study.

## References

1. J. H. BROWN, *Mag. Conc. Res.* **12** (1972) 185.
2. G. A. COOPER and J. FIGG, *J. Brit. Ceram. Soc.* Jan (1972) 104.
3. H. G. ALLEN, *Composites* **2** (1971) 98.
4. M. A. ALI, A. J. MAJUMDAR and B SINGH, *J. Mater. Sci.* **10** (1975) 1732.
5. C. E. INGLIS, *Trans. Inst. Naval Archit.* **55** (1913) 219.
6. A. A. GRIFFITH, *Phil Trans. Roy. Soc. 1* **221** (1920) 163.
7. G. R. IRWIN, *Appl. Mater. Res.* (1964) 65.
8. G. I. BARENBLATT, *Adv. Appl. Mech.* 7 (1962) 55.
9. J. M. KRAFFT, A. M. SULLIVAN and R. W. BOYLE, Proceedings of the Crack Propagation Symposium, Vol 1. (Cranfield, England, 1961). 8–26.
10. J. I. BLUHM, "Fracture 5" Edited by H. Liebowitz, (Academic Press, New York, 1968) Ch. 1.
11. J. H. BROWN, *Mag. Conc. Res.* **25** (1973) 31.
12. P. C. PARIS and G. C SIH, *ASTM STP* **381** (1964) 67.
13. H. KRENCHEL, "Fibre reinforcement", (Akademic Forlag, Copenhagen, 1964)
14. R. D. De VEKEY and A. J. MAJUMDAR, *Mag. Conc. Res.* **20** (1968) 229.

Received 21 March and accepted 6 July 1978.